Applied Catalysis B: Environmental 148–149 (2014) 573–581

Contents lists available at ScienceDirect

Applied Catalysis B: Environmental

journal homepage: www.elsevier.com/locate/apcatb

Nitric oxide oxidation catalyzed by microporous activated carbon fiber cloth: An updated reaction mechanism

Zhanquan Zhang[a,b,c], John D. Atkinson[b], Boqiong Jiang[d], Mark J. Rood[b,*], Zifeng Yan[a,**]

[a] State Key Laboratory of Heavy Oil Processing, Key Laboratory of Catalysis CNPC, China University of Petroleum, Qingdao 266580, China
[b] Department of Civil and Environmental Engineering, University of Illinois at Urbana-Champaign, 205 N. Mathews Avenue, IL 61801, USA
[c] College of Mechanical and Electrical Engineering, China University of Petroleum, Qingdao 266580, China
[d] College of Environmental Science and Engineering, Zhejiang Gongshang University, Hangzhou 310012, China

ARTICLE INFO

Article history:
Received 14 August 2013
Received in revised form 22 October 2013
Accepted 26 October 2013
Available online 2 November 2013

Keywords:
NO oxidation
Activated carbon
Oxidation mechanism
NO_2 sorption

ABSTRACT

New catalysts, in particular activated carbons, are being developed to improve NO oxidation kinetics and to minimize the negative impacts of water vapor and SO_2 as an alternative NO_x control strategy for flue gases. However, the literature is inconclusive about the pathway to achieve a stable downstream NO_2 concentration, creating discrepancies in the NO oxidation mechanism. In this paper, a simple two-step mechanism is proposed and justified for NO oxidation catalyzed by microporous activated carbon. In the first mechanistic step, NO is rapidly oxidized to NO_2 in activated carbon's micropores with constant NO conversion efficiency, *prior* to the formation of adsorbed intermediates (e.g., $C^*—NO_2$, $C^*—NO_3$ or $C^*—NO—NO_3$). This conclusion challenges the idea that NO oxidation to NO_2 requires decomposition of the $C^*—NO—NO_3$ intermediate. Instead, we show that the physical properties of the catalyst (i.e., micropore width and volume) control steady-state NO oxidation kinetics, with carbon's chemical properties having no apparent impact for the conditions tested here. In the second mechanistic step, newly formed NO_2 is chemically adsorbed on the carbon surface, resulting in formation of NO and C—N or C—O complexes. Chemical disproportion of NO_2 proceeds until the carbon surface is saturated with these complexes. It follows that the first step of the mechanism (NO oxidation in micropores) controls steady state NO oxidation kinetics while the second step (NO/carbon surface reactions) controls transient NO oxidation kinetics. This two-step mechanism is confirmed via in situ cyclic experiments and NO_2 pre-adsorption tests. Pre-saturation of the carbon surface with functional groups decreases the impact of the second mechanistic step, affecting transient NO oxidation kinetics but having no impact on steady-state oxidation kinetics. A more complete understanding of the reaction mechanism allows us to better prepare tailored carbonaceous NO oxidation catalysts.

1. Introduction

Emissions of nitrogen oxides (NO_x) from anthropogenic activities contribute to acid rain, ozone depletion, photochemical smog, secondary pollutants, and respiratory diseases [1–3]. Nearly all anthropogenic NO_x (95%) derives from transportation (49%) and electricity generation (coal-fired power plants, 46%) [4]. It is important to improve existing NO_x control strategies with world coal consumption expected to increase 60% by 2030 [5] and with the implementation of more stringent NO_x emission regulations, including the US EPA's 2011 Cross State Air Pollutant Rule and China's 2012 Emissions Standards [6,7]. The leading post-combustion technology for NO_x abatement is selective catalytic reduction (SCR), which may experience ammonia penetration to the atmosphere, N_2O formation at high temperatures (300–400 °C), and increased operating costs associated with gas reheating and catalyst deactivation by SO_2 and alkali metals [8].

Catalytic oxidation of NO ($2NO + O_2 \rightarrow 2NO_2$) over microporous activated carbon combined with subsequent absorption of NO_2 as a more soluble NO_x specie is an alternative to SCR. Compared with SCR, carbon catalyzed NO oxidation operates at low temperatures (<100 °C) and could potentially be used for simultaneous control of multiple pollutants [9]. While this research combines NO oxidation with NO_2 absorption, a thorough understanding of carbon-catalyzed NO oxidation can also be important for improving NO reduction via fast SCR reactions [10,11]. Since Mochida's initial studies introducing carbon-catalyzed NO oxidation, extensive effort has been placed on understanding the reaction mechanism. After 20 years, however, the mechanism continues to be debated

* Corresponding author. Fax: +1 217 333 9464.
** Corresponding author. Fax: +86 532 86981295.
E-mail addresses: mrood@illinois.edu (M.J. Rood), zfyancat@upc.edu.cn (Z. Yan).

0926-3373/$ – see front matter © 2013 Elsevier B.V. All rights reserved.
http://dx.doi.org/10.1016/j.apcatb.2013.10.050

[12–15]. The complexity of activated carbon (i.e., variability in the activated carbon's physical and chemical properties) and NO auto-oxidation [16] make characterizing the NO oxidation mechanism challenging. Recent studies investigating the impacts of chemical functionalities on NO oxidation show that oxygen functional groups impact NO_2 adsorption capacity and transient oxidation kinetics [17–19].

The kinetics of heterogeneous catalysis depend on: (1) reactant adsorption, (2) catalytic reaction at active sites, and (3) product desorption. The reaction rate, therefore, is influenced by the physical and chemical properties of the catalyst [20]. Proposed mechanisms for carbon catalyzed NO oxidation are summarized as follows. Mochida [12–14] first investigated the influence of carbon's physical and chemical properties, as well as process parameters (e.g., NO and O_2 concentrations, reaction temperature, and gas hourly space velocity), on steady-state NO oxidation kinetics. Mochida suggested that $[NO{-}O{-}NO_2]_{ad}$ is a crucial intermediate for NO_2 formation/desorption and that NO adsorption is the rate-determining step due to competition with desorbed NO_2 and intermediates [13]. This proposed mechanism, consistent with observed kinetic profiles, suggests that $(NO)_2$, NO_2, and $(NO_2)_2$ are not necessary as reaction intermediates [21]. Adapa [15] more recently proposed Langmuir–Hinshelwood (L–H) and Eley–Rideal (E–R) mechanisms for carbon-catalyzed NO oxidation. In the L–H mechanism, dissociated oxygen activated by carbon reacts with adsorbed NO. In the E–R mechanism, gaseous O_2 directly reacts with NO adsorbed in micropores. Both mechanisms, though fundamentally different, rely on the evolution of similar reactive intermediates, including $C^*{-}NO$, $C^*{-}NO_2$, $C^*{-}NO_3$ and $C^*{-}NO{-}NO_3$. Predictions based on Adapa's transport model and proposed mechanism fit well with experimental data when considering NO release from intermediates and regeneration of the activated carbon's active sites. Later, Zhang [17,22] proposed that NO_2, formed via NO oxidation, decomposes and causes rapid oxidation of the carbon surface with subsequent NO_2 chemisorption. In our recent paper, we extended this concept by identifying and quantifying these generated oxygen groups, highlighting their contribution toward the carbon catalyst's acidity and describing their impact on transient NO oxidation kinetics [19].

To date, all proposed NO oxidation mechanisms stress the importance of carbon's catalytic sites, the number of which should, in theory, be proportional to carbon's accessible surface area. The literature, however, indicates that steady-state NO oxidation kinetics are independent of carbon's accessible surface area [14]. Furthermore, steady-state NO conversion efficiency increases with increasing NO concentration ([NO]). This Langmuir-type dependence on [NO] supports that the reaction is not limited by the availability of active sites. This is the opposite of SCR systems [23] and metal oxide catalyzed NO oxidation, where steady-state NO conversion efficiency is inversely proportional to [NO] [24]. Continued investigation into carbon-catalyzed NO oxidation is necessary to address the role of carbon's physical and chemical properties on transient and steady-state oxidation kinetics.

The goal of this paper is to provide an updated NO oxidation reaction mechanism. To achieve this goal, in situ cyclic experiments and NO_2 pre-adsorption tests are used. We propose and justify that carbon surface saturation due to NO_2 sorption controls transient NO oxidation kinetics, including the time required to achieve a steady effluent $[NO_2]$. Our updated NO oxidation mechanism consists of two consecutive steps: (1) NO_2 is rapidly formed through gas phase reactions between NO and O_2 in micropores; formation and decomposition of $C^*{-}NO_x$ species, as has been previously postulated [13], does not occur, and (2) newly formed NO_2 adsorbs to the carbon surface and is associated with NO_2 reduction and development of $C^*{-}NO_x$ and $C^*{-}O$ functionalities. The physical properties of the activated carbon control steady-state NO oxidation kinetics, and carbon's adsorption and surface reaction tendencies impact transient conversions by allowing for destruction of the NO_2 product and regeneration of the NO reactant. The second mechanistic step diminishes as the carbon surface saturates with adsorbed NO_x species and oxygen functionalities. At steady-state, the carbon surface is saturated, preventing further NO_2 reduction.

2. Methods

2.1. NO oxidation experiments

Air (99.9995%), nitrogen (99.999%), certified 1000 ppm_v NO in N_2, and certified 970 ppm_v NO_2 in N_2 were used as purchased from S.J. Smith, Inc. Mass flow controllers controlled the flow rate for each gas, and a controlled temperature water bath maintained the reaction temperature. NO oxidation experiments were performed at 50 °C in a stainless steel fixed-bed reactor (inner diameter 0.926 cm, outer diameter 1.244 cm), packed with 0.25 g of Novoloid-based Activated Carbon Fiber Cloth (ACFC-10: American Technical Trading, Inc., lot #: ACC-5092-10, bed length: 0.8 cm, gas hourly space velocity: $1.2 \times 10^4\ h^{-1}$) with a total inlet gas flow rate of 0.1 standard liters per minute (SLPM, standard conditions are 0 °C and 1 atm) [18]. Unless otherwise noted, the reactant gas was 380 ppm_v NO, 10 vol% O_2, and balance N_2. A bypass line to the downstream NO_x detector ensured stable NO_x concentrations prior to experiments and a blank experiment confirmed that non-catalyzed NO oxidation was minimal (<2% for all conditions tested herein). Outlet [NO], $[NO_2]$ and $[NO_x]$ were measured and recorded every 10 s with a $NO{-}NO_2{-}NO_x$ analyzer (Thermo Scientific, 42i-HL). For all experiments, inlet and effluent $[NO_x]$ were equal (±1%) at steady-state. Steady-state NO conversion efficiency (%) was calculated as follows:

$$NO_{conversion} = \frac{[NO]_{inlet} - [NO]_{effluent}}{[NO]_{inlet}} \times 100\% \quad (1)$$

where $[NO]_{inlet}$ and $[NO]_{effluentt}$ are the inlet and effluent NO concentrations (ppm_v), respectively.

2.2. NO oxidation cycle experiments

Cycle experiments included NO oxidation followed by select regeneration strategies (Fig. S1). NO oxidation occurred as described above. For regeneration by purging, 0.08 SLPM of N_2 purged the vessel at 50 °C for 20 h. For regeneration by temperature-programmed desorption (TPD), 1 SLPM of N_2 passed through the reactor as the temperature increased from 25 °C to 300 °C at 5 °C min^{-1}. Heating stopped and the reactor was immediately cooled in N_2 after reaching 300 °C. Heating tapes (Omega, FGS101-060) with a proportional–integral–derivative (PID) controller (Omega, CNi16) controlled temperatures during TPD. All spent carbons were collected and stored in glass vials purged with N_2.

Carbon's NO_x adsorption capacity was calculated as follows:

$$Q_{ads} = \frac{F \times \int_0^{\infty} ([NO_x]_{inlet} - [NO_{x_{effluent}}])dt}{m_{carbon} \times V_m} \quad (2)$$

where Q_{ads} is carbon's NO_x capacity (μmol NO_x per g carbon, μmol g^{-1}), F is the total gas flow rate (L h^{-1}), $[NO_x]_{inlet}$ and $[NO_x]_{effluent}$ are the inlet and effluent NO_x concentrations (ppm_v), respectively, m_{carbon} is the mass of activated carbon catalyst (g), and V_m is the standard molar volume of gas (L mol^{-1}).

2.3. NO_2 pre-sorption experiments

To saturate the carbon with adsorbed NO_x species, the carbon was exposed to 0.1 SLPM of 970 ppm_v NO_2 (in N_2) at 50 °C.

Pre-sorption stopped when the outlet [NO] was < 20 ppm_v (note that NO_2 reduction to NO by carbon occurs, as described in [22]). Carbon was assumed to be saturated with NO_x at this time. After NO_2 pre-sorption, the carbon was purged with 0.08 SLPM N_2 at 50 °C for > 12 h to remove weakly adsorbed species and then tested for NO oxidation.

2.4. Characterization

N_2 sorption measurements were carried out at −196 °C with a surface analyzer (Micrometrics, ASAP 2010). Prior to analysis, carbon samples were degassed under vacuum (500 μm Hg) for >16 h at 150 °C. BET surface area (S_{BET}) was calculated from relative pressures (P/P_0) between $0.005 < P/P_0 < 0.1$, and the total pore volume was recorded at $P/P_0 = 0.98$. Micropore volume (V_{micro}), total pore volume (V_{total}), and average micropore width (D_{micro}) were calculated using the 3D model [25]. Carbon's surface coverage with adsorbed NO_2 is calculated using the catalyst's BET surface area and assuming NO_2 molecules are spherical (3.4 Å diameter).

Bulk elemental composition (C, H, N, and O) was determined at the University of Illinois Urbana-Champaign's (UIUC's) Chemistry Microanalysis Lab with a CE-400 Elemental Analyzer (Exeter Analytical, Inc.). Surface functional groups on the carbon samples were determined with X-ray photoelectron spectroscopy (XPS) using a Kratos Axis Ultra spectrometer. All binding energies were calibrated to a C1s peak located at 284.8 eV. Peak fittings were obtained using the Gaussian–Lorentzian (30%) equation and assuming constant full width at half maximum (FWHM) for all peaks. Adsorbed species were also identified with Fourier transform infrared spectroscopy (FTIR, Thermal Nicolet NEXUS 670) using the KBr wafer technique with a concentration of 1 wt% carbon in KBr, 50 scans, and 2 cm^{-1} resolution. Surface morphology of ACFC-10 was observed using scanning electron microscopy (SEM, Hitachi, S-4700) with an accelerating voltage of 10 kV.

3. Results and discussion

The physical and chemical properties of virgin ACFC-10 are summarized in Table 1. Virgin ACFC-10 has a narrow pore width centered at 6.69 Å and microporosity is 98% (Table 1). It has a high carbon content (93.95%) without ash [26]. These characteristics not only facilitate NO oxidation [17], but also prevent catalytic interference and unwanted reactions [27], allowing for isolation of carbon's impact on NO oxidation. Fig. S2 shows the physical morphology of virgin ACFC-10, with arithmetic mean fiber diameter of 13.8 μm.

3.1. NO oxidation cycle experiments

Results for a blank experiment, showing that uncatalyzed NO oxidation is 1.6%, are included in Fig. S3. For carbon-catalyzed NO oxidation, the kinetic profiles for [NO] and [NO_2] during Cycle 1 (Fig. 1a) are consistent with the literature [12–14]. ACFC-10 can oxidize 57% of NO to NO_2, and increased NO conversion efficiency could be achieved by increasing the mass of carbon or the inlet concentration of NO, as has been described in the literature [14]. For this paper, intermediate conversion efficiencies are used so that the impacts of the catalyst's properties on transient and steady-state NO oxidation kinetics can be identified. During this cycle, [NO] rapidly (within 6 min) decreases toward 100 ppm_v due to NO adsorption [29,30], then increases to 220 ppm_v after 10 min because of carbon's limited adsorption capacity for NO (Fig. 1a is provided with higher temporal resolution in Fig. S4). This rapid [NO] increase after 10 min represents breakthrough. Afterwards, there is an initial decrease to 190 ppm_v after 20 min, a gradual increase to a peak value of 240 ppm_v (6.2 h), and then a slow but progressive decrease to the steady-state concentration of 164 ppm_v. NO_2 breakthrough begins after 3.1 h. At steady-state, NO_x adsorption capacity is 1594 μmol g^{-1}, which corresponds to 8.7% surface coverage and is representative of the NO oxidation conditions used in this manuscript (Table 3).

Upon achieving steady-state NO conversion ([NO] change < 1 ppm_v h^{-1}), ACFC-10 was purged with N_2 at 50 °C to regenerate the catalyst. During the purge, 358 μmol g^{-1} of NO_x, consisting of 323 μmol g^{-1} of NO_2 and 35 μmol g^{-1} of NO, desorbed (Fig. S5). Consistent with the literature, we attribute this to decomposition of $C^*—ONO_2$ and $C^*—NO_2$, releasing NO_2 and NO, respectively, and suggesting that $C^*—ONO_2$ is the dominant species [31]. Purging at 50 °C only desorbs weakly adsorbed compounds, as evidenced by the difference between total NO_x adsorbed during NO oxidation (1594 μmol g^{-1}) and desorbed during purging (358 μmol g^{-1}).

The N_2 purged sample was reused as an NO oxidation catalyst (Cycle 2), and distinct differences between the two cycles are evident. For Cycle 2, NO_2 breakthrough occurs immediately and [NO_2] increases more rapidly, the [NO] peak is lower (180 ppm_v) and occurs sooner, and the system achieves steady-state conditions 78% faster than Cycle 1 (Fig. 1a). The NO_x sorption capacity (Q_{NO_x}) during oxidation Cycle 2 is 300 μmol g^{-1}, which is similar to the amount desorbed during purging (358 μmol g^{-1}). Despite the obviously different pathways to achieving steady-state, both cycles have identical NO conversion efficiencies once the concentrations have stabilized. In other words, transient NO oxidation kinetics are highly variable for the two cycles, while steady-state NO oxidation kinetics are constant. N_2 purging after Cycle 2 desorbs 315 μmol g^{-1} of NO_x and the desorption profile is consistent with Cycle 1 (Table 2).

TPD was used to identify strongly adsorbed species that remained on the Cycle 2 carbon catalyst after purging (Fig. 2a). 1220 μmol g^{-1} NO_x desorbed, including 523 μmol g^{-1} NO and 697 μmol g^{-1} NO_2 (Table 2), completing the NO_x balance and indicating that all adsorbed species were removed during regeneration. This is corroborated by FTIR, which shows no peaks associated with nitrites or nitrates after TPD (Fig. 2c). During TPD, NO_2 desorption starts at 50 °C, approximately 40 °C before NO desorption, and the maximum release rates of NO_2 and NO occur at 120 °C and 145 °C. These temperatures are consistent with TPD profiles for carbon pre-treated with NO_2 [12,22,31] (Fig. 2b), suggesting that adsorbed species are similar during NO oxidation and NO_2 sorption. NO and NO_2 release during TPD originates from the decomposition of adsorbed nitrogen containing species, as confirmed with an FTIR signal at 1380 cm^{-1} (NO_3^-) (Fig. 2c) and an XPS signal at 406 eV (NO_3^-) (Fig. 2d) [32]. For ACFC-10 pretreated with NO_2, the same FTIR (Fig. 2c) and XPS (Fig. 2d) peaks are observed.

After TPD, a final NO oxidation cycle was completed (Cycle 3). [NO] and [NO_2] profiles for Cycle 3 resemble Cycle 1, but the NO_2 breakthrough time and the time to achieve steady-state is notably improved despite the absence of adsorbed nitrogen-containing species. Compared to Cycle 1, there is a 55% reduction in NO_2 breakthrough time and a 61% reduction in time to reach steady-state. The NO_x adsorption capacity is reduced by 33% to 1061 μmol g^{-1} from 1594 μmol g^{-1} for Cycle 1 with a peak [NO] of 210 ppm_v for Cycle 3 compared to 240 ppm_v for Cycle 1 (Table 2). As seen with Cycle 2, despite changing transient NO oxidation kinetics, steady-state kinetics, including NO conversion efficiency, are constant (Table 1).

Published mechanisms propose that NO_2 formation is caused by decomposition of adsorbed $C^*—NO—NO_3$ species or $[NO—O—NO_2]_{ad}$ multi-molecular intermediates [13,15]. The rate determining step in these mechanisms is the decomposition of the adsorbed species or intermediates [15]. It would be expected that steady-state NO conversion efficiency should be proportional to the quantity of these adsorbed species, as has been shown for NO oxidation catalyzed by metal oxides [33] and SCR catalyzed by iron titanate [34].

Table 1
Physical and chemical properties of virgin ACFC-10 and ACFC-10 after two sequential oxidation cycles followed by thermal regeneration (CY-2).

Samples	Physical properties				Chemical properties							
	S_{BET}/m^2 g^{-1}	D_{micro}/Å	V_{total}/cm^3 g^{-1}	V_{micro}/cm^3 g^{-1}	Bulk element/wt%			Surface atomic concentrations/atom%				
					C	H	O	C—Ar & C—Al[a]	C—O	C=O	COOH	Carbonates or CO_2 [b]
ACFC-10	1000	6.69	0.410	0.402	93.95	0.83	5.09	72.9	14.3	5.66	3.92	3.30
Cycle 2[c]	994	6.62	0.435	0.412	91.57	0.71	7.25	76.6	10.3	5.78	3.76	3.59

[a] C—Ar, aromatic carbon bonds; C—Al, aliphatic carbon bonds.
[b] This peak may be attributed to the shake-up satellite (π–π^*). Note that differentiating between carbonates and CO_2 was also not possible [28].
[c] The samples after Cycle 1 and Cycle 3 are not shown because of the presence of unstable adsorbed species.

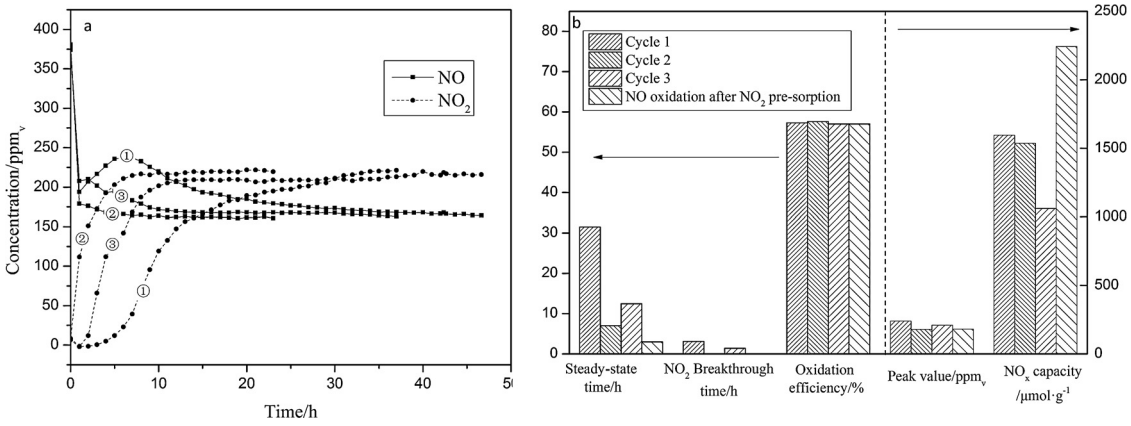

Fig. 1. (a) Effluent profiles of [NO] and [NO_2] during NO oxidation cycles (the cycle number is indicated on each profile), (b) comparison of kinetic parameters and steady-state NO conversion efficiency for NO oxidation cycles and NO oxidation after pre-treating the carbon catalyst with NO_2.

Table 2
NO_x adsorption capacities and relevant kinetic parameters for three NO oxidation cycles. NO_x desorption is also quantified for post-oxidation regeneration.

	NO oxidation				Regeneration			
	Cycle 1	Cycle 2	Cycle 3		Cycle 1-purge	Cycle 2-purge	Cycle 2-TPD	Cycle 3-purge
Q_{NO_x}/μmol g^{-1}	1594	300	1061	Q_{NO_x}/μmol g^{-1}	358	315	1220	283
t_{NO_2}/h[a]	3.1	0	1.4	Q_{NO}/μmol g^{-1}	35	23	523	23
t_{steady}/h[b]	31.5	7	12.5	Q_{NO_2}/μmol g^{-1}	323	291	697	260
[NO] peak/ppmv	240	180	210					
Conversion/%	57.3 ± 0.86	57.6 ± 0.37	57					

[a] t_{NO_2} is the time from the start of NO oxidation until an outlet concentration of 1 ppmv NO_2 is achieved.
[b] t_{steady} is the first time when the change in [NO] is < 1 ppmv h^{-1}.

Our results show that this mechanism cannot extend to carbon-catalyzed NO oxidation, because steady-state NO oxidation kinetics are independent of the amount of adsorbed NO_x (Fig. 1b, Fig. S6 and Table 2). This is consistent with our previous publication that describes constant steady-state NO oxidation kinetics during four consecutive cycles despite carbon's decreasing NO_x capacity [19]. We have also shown that surface functional groups (C*—O) do not influence steady-state NO oxidation kinetics. The catalyst in Cycle 3 is expected to have notably more oxygen content than the catalyst in Cycle 1. While this additional oxygen decreases the NO_x adsorption capacity of the carbon and therefore alters the transient NO oxidation kinetics, it has no impact on steady-state kinetics. For this system, steady-state NO oxidation kinetics are not impacted by the carbon's NO_x adsorption capacity or surface functional groups, and

Table 3
NO_2 adsorption capacities for select gas conditions.

	970 ppmv NO_2 + N_2	220 ppmv NO_2 + N_2	220 ppmv NO_2 + 10% O_2 + N_2	220 ppmv NO_2 + 164 ppmv NO + N_2 [d]	0 ppmv NO_2 + 380 ppmv NO + 10% O_2 + N_2
NO_x capacity/μmol g^{-1}	3052	1850	1650	1452	1594
Surface coverage/%	16.7	10.1	9.0	7.9	8.7
Purge desorption/μmol g^{-1}	861	N/A[a]	N/A	N/A	358
[NO] peak/ppmv	550	134	95	129 + 164[b]	76 + 164[c]

[a] N/A, not applicable because purge step was not applied after the reaction.
[b] 164 ppmv is the initial [NO] of inlet gas.
[c] 164 ppmv is the value of [NO] of outlet gas after reaching steady-state conditions during NO oxidation.
[d] To simulate the steady-state conditions observed during NO oxidation, a controlled gas stream consisting of 164 ppmv NO and 220 ppmv NO_2 was injected into the fixed bed.

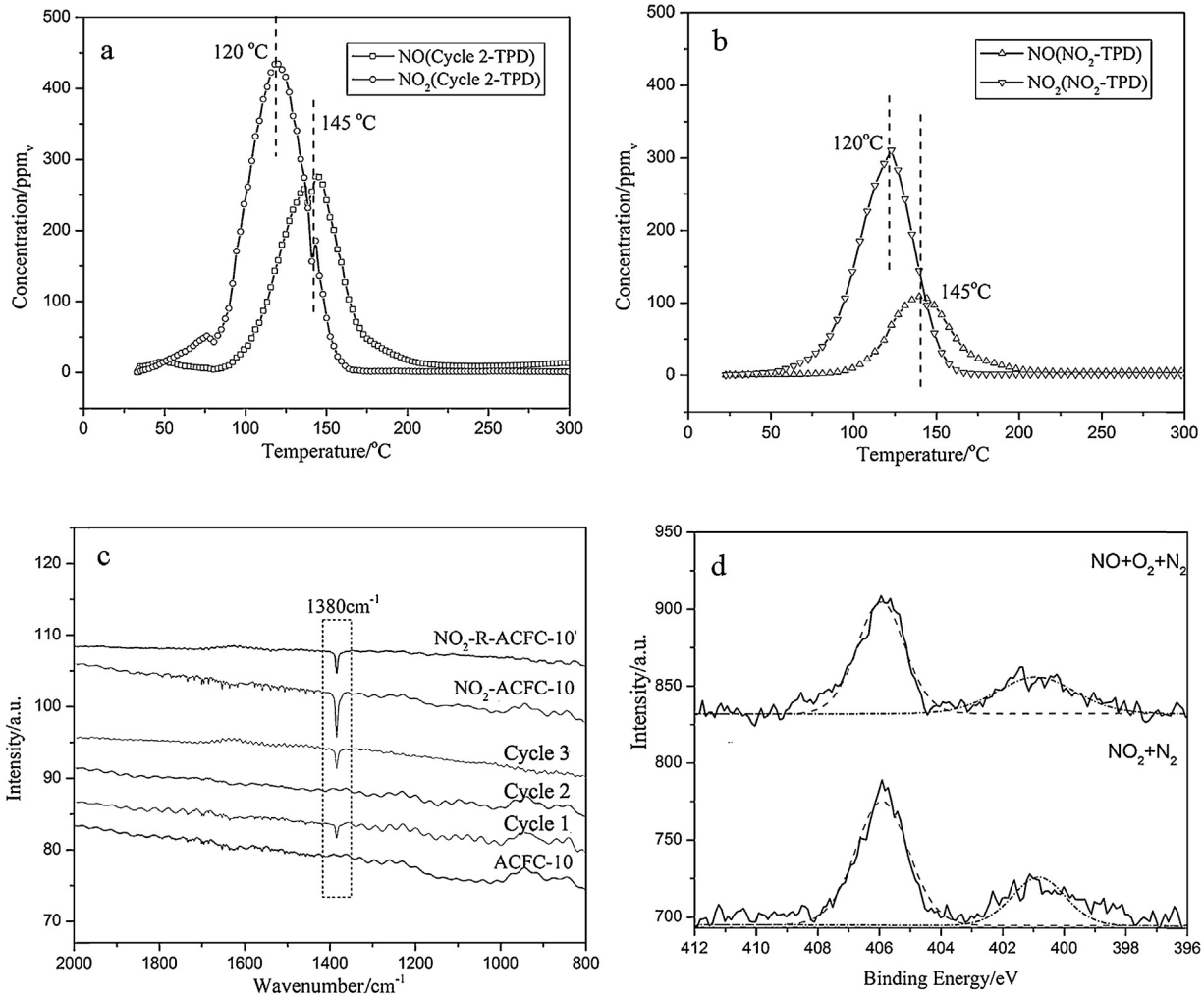

Fig. 2. (a) Effluent [NO], [NO_2], and [NO_x] profiles during TPD for the Cycle 2 carbon; (b) effluent [NO], [NO_2] and [NO_x] profiles during TPD for carbon treated with 220 ppm_v NO_2; (c) FTIR spectra for NO oxidation cycle carbons and carbons treated with NO_2 (before and after purging); (d) XPS spectra for ACFC-10 after NO oxidation and purging, or NO_2 treatment (970 ppm_v) and purging.

the carbon-catalyzed NO oxidation mechanism should be updated to account for these findings.

Carbon's physical properties, chemical properties, and adsorbed species should be considered to develop this updated reaction mechanism. When adsorbed NO_x species are present, it is difficult to assess the activated carbon's physical properties. For N_2 adsorption measurements, pre-heating under vacuum desorbs NO_x from activated carbon, and N_2 adsorption at −196 °C may condense NO_2 (melting point (m.p.)NO_2 = −11.2 °C, 1 atm) or NO_2—NO_2, blocking micropores [35,36]. Hence, Table 1 only describes physical properties for those samples believed to be stable under modest heating (150 °C) and vacuum (500 μm Hg) (virgin ACFC-10 and Cycle 2).

Physical and chemical properties of virgin ACFC-10 and CY-2 are described in Table 1 and Fig. 3. The carbons have similar physical properties, but the Cycle 2 carbon has 42% more bulk oxygen content. Oxygen is deposited onto carbon from decomposition of C*—ONO_2 and C*—NO_2 during TPD [22,31,37], though this regeneration does not influence the carbon's physical properties (e.g., pore size and pore volume). The change in oxygen content has no apparent influence on steady-state NO oxidation kinetics, which contradicts recent publications [15,38].

Zigzag and armchair edge sites of activated carbon are possible NO adsorption sites, favoring an adsorption configuration with the nitrogen atom in the downward orientation, toward the carbon [39]. Since steady-state NO conversion efficiency is not proportional to accessible surface area, these sites are not expected to be catalytically active for NO oxidation [14].

Summarizing our findings to this point, steady-state NO oxidation kinetics for microporous activated carbon are independent of surface and bulk oxygen, adsorbed NO_x species, and the number of available zigzag or armchair edge sites. Saturating the carbon's surface with NO_x allows the system to more rapidly achieve steady-state, without changing the steady-state oxidation kinetics. Since NO and O_2 have low affinity for carbon [40], NO_2 dominates the adsorbed species. We hypothesize, therefore, that NO_2 adsorption controls transient NO oxidation kinetics without impacting steady-state kinetics [22,31].

3.2. NO_2 sorption

Our hypothesis that transient NO oxidation kinetics are controlled by the interaction between newly formed NO_2 and carbon's surface was evaluated by pretreating the catalyst with 970 ppm_v NO_2. The saturated carbon was then used for NO oxidation, assessing the impact of adsorbed species on transient NO oxidation kinetics (e.g., NO_2 breakthrough time and time required to achieve steady-state). During the first several hours of NO_2 treatment, effluent [NO_2] is low (70 ppm_v) while [NO] increases sharply, reaching 520 ppm_v after 3 h (Fig. 4). After reaching its peak, [NO] decreases asymptotically toward zero as outlet [NO_2] increases

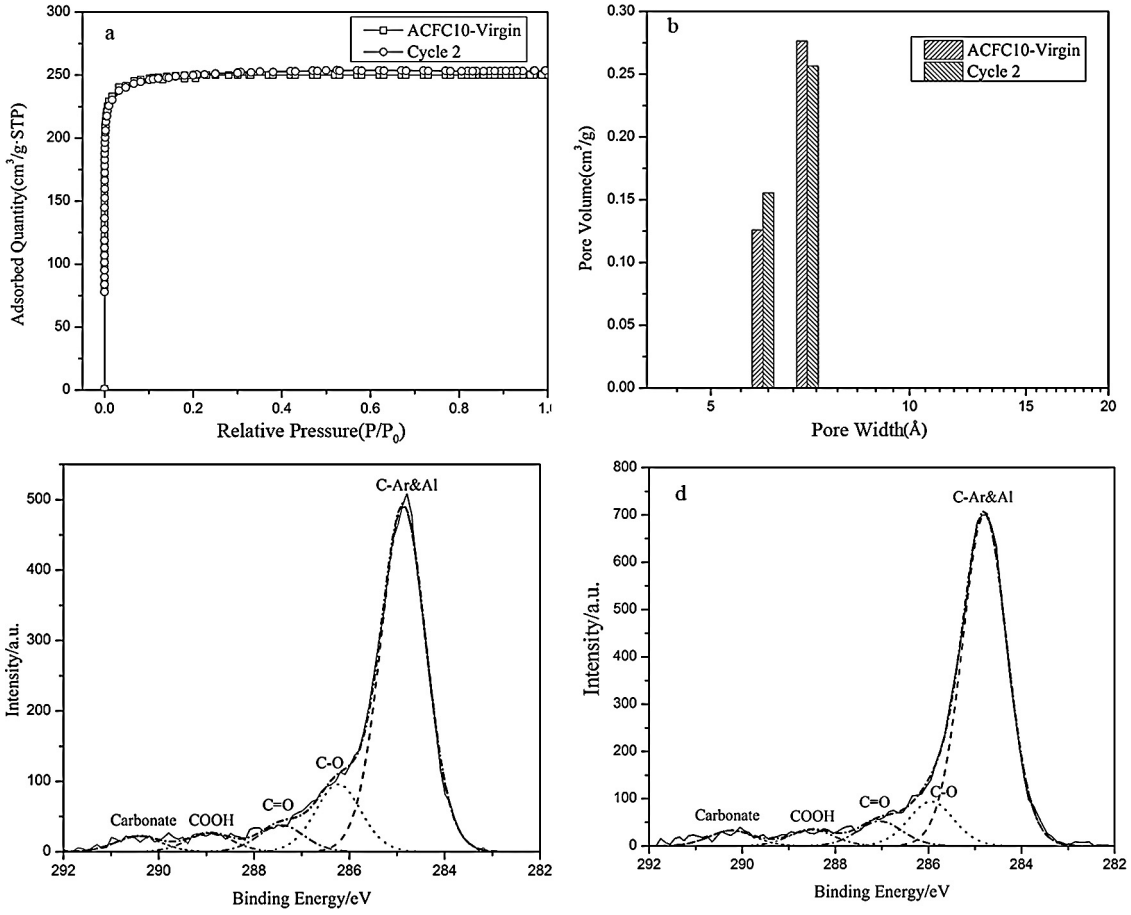

Fig. 3. (a) N_2 adsorption isotherms for virgin ACFC-10 and Cycle 2 carbon after purging and TPD; (b) pore size distribution for virgin ACFC-10 and Cycle 2 carbon; C1s XPS spectrum for (c) virgin ACFC-10 and (d) Cycle 2 carbon.

toward its inlet value. Total NO_x adsorption during this treatment is 3052 μmol g^{-1}. Compared to Cycle 1 (1594 μmol g^{-1}), more NO_x is adsorbed here because the carbon is exposed to higher concentrations of NO_2 (970 ppm_v compared to 220 ppm_v). Observed trends during NO_2 sorption are consistent with the literature [19,37,41], including NO_2 reduction by carbon that results in NO formation.

Purging the NO_2-treated activated carbon with N_2 at 50 °C desorbs 861 μmol g^{-1} of NO_x. After purging, the carbon was tested as an NO oxidation catalyst. Steady-state, including 57% NO conversion efficiency, is achieved within 3 h (57% faster than Cycle 2) and is accompanied by low NO_x adsorption capacity (52 μmol g^{-1}) (Fig. 4b). More adsorbed NO_x on the carbon catalyst decreases the time required to achieve steady-state despite having no noticeable impact on steady-state NO oxidation kinetics, confirming that NO_x sorption controls the transient NO oxidation kinetics of the catalyst.

An FTIR peak at 1380 cm^{-1} and an XPS peak at 406 eV, attributed to NO_3^- on the surface of carbon, are observed for carbon after NO oxidation and NO_2 pre-sorption. This is consistent with previously

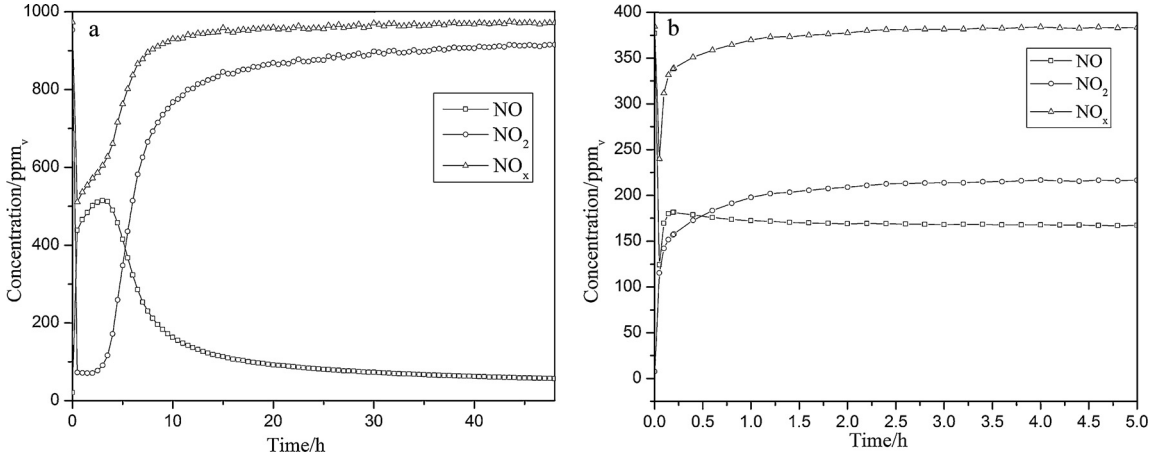

Fig. 4. Effluent [NO], [NO_2], and [NO_x] profiles during: (a) NO_2 adsorption and (b) during subsequent NO oxidation preceded by N_2 purge.

published research showing that NO_2 is the oxygen source for surface functionalities formed during both NO_2 and $NO + O_2$ sorption on carbon films [42,43]. It is speculated that these atmospheres provide similar environments for developing surface functionalities on activated carbon.

These results indicate that carbon surface saturation occurs during NO oxidation due to adsorption of newly formed NO_2. For a carbon pre-saturated with NO_2, steady-state is achieved rapidly. Adsorbed species are *not* precursors or intermediates that must be consumed to generate NO_2, as others have suggested [13,15]. Instead, NO_2 directly forms in the carbon's micropores from gas phase reactions between NO and O_2 and adsorbed species are generated *after* NO_2 formation. Furthermore, for a single carbon catalyst with stable physical properties, changing the NO_x adsorption capacity does not affect steady-state NO oxidation kinetics, again highlighting that NO_2 formation is independent of adsorbed NO_x species. These results are the first demonstration that NO_2 formation during carbon-catalyzed NO oxidation occurs prior to, and independent from, the generation of adsorbed NO_x species.

3.3. Proposed mechanism for carbon-catalyzed NO oxidation

The carbon-catalyzed NO oxidation mechanism should be divided into two consecutive components: Step 1 – NO_2 formation via NO oxidation in activated carbon's micropores, and Step 2 – reactive adsorption of NO_2 onto activated carbon's surface. Step 1 stabilizes rapidly, but steady-state NO oxidation kinetics are not observed until Step 2 results in saturation of the carbon's NO_2-active sites. Transient NO oxidation kinetics, including the time required to achieve steady-state, depend on the NO_2 sorption capacity of the activated carbon, but this property has no impact on the steady-state performance of the catalyst. Identical steady-state NO conversion efficiencies are achieved slowly for a fresh carbon catalyst and more rapidly for a carbon pre-saturated with NO_2. Effluent NO observed during the early stages of NO oxidation is attributed to un-reacted NO associated with Step 1 of the reaction mechanism and NO formed via NO_2 reduction by carbon in Step 2 of the mechanism. Steady-state conditions occur when the NO contribution from Step 2 is zero. Correspondingly, effluent NO_2 observed before steady-state conditions consists only of NO_2 that is formed via Step 1 and not consumed during Step 2. At steady-state, all effluent NO_2 results from Step 1 since adsorption/reaction via Step 2 cannot occur on the saturated carbon surface. Such conclusions explain the observed variability in transient NO oxidation kinetics, and it is believed that only the carbon's physical properties control the steady-state NO oxidation kinetics.

The literature concludes that NO oxidation is second order in [NO], with 10 vol% oxygen representing a reactant excess compared to 400 ppm_v NO [12,44]. The reaction rate (r[NO]) can be expressed as follows, with k as the apparent reaction rate:

$$r[\mathrm{NO}] = k[\mathrm{NO}]^2 \tag{3}$$

Assuming a fixed-bed, plug flow reactor with negligible diffusion limitations, NO conversion (X%) in Step 1 of the updated NO oxidation reaction mechanism can be expressed as a function of catalyst bed length (L, cm), based on the pseudo second-order rate equation for integral reactors [42].

$$X\% = 100 \times \left(1 - \frac{F_{A0}}{kC_0^2 \rho \times S \times L + F_{A0}}\right) \tag{4}$$

where C_0 is the inlet [NO] ($mol\,cm^{-3}$), F_{A0} is the NO feed rate ($mol\,h^{-1}$), ρ is the packing density of catalyst bed ($g\,cm^{-3}$), and S is the cross sectional area of the reactor (cm^2). An outlet [NO] of 164 ppm_v should be achieved in 0.3 s (contact time) for our experimental conditions (L = 0.8 cm, $F_{A0} = 1.018 \times 10^{-4}$ $mol\,h^{-1}$). The intent of using this model with, rather extreme, assumptions is to only compare the ideal timescale for achieving steady NO_2 concentration (<1 s) to what is observed in experiments (often, >24 h).

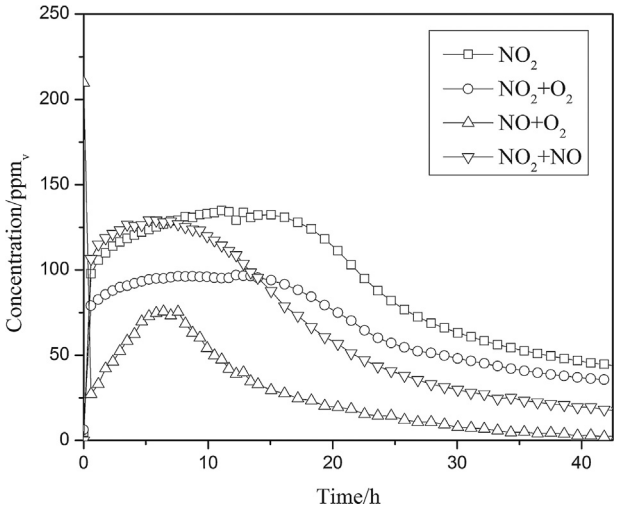

Fig. 5. Effluent [NO] profiles during NO_2 sorption over carbon in select atmospheres. [NO] during for ($NO + O_2$) and ($NO + NO_2$) are offset by 164 ppm_v to isolate NO generated by NO_2 reduction (as opposed to unreacted NO).

Steady [NO] (164 ppm_v) is achieved after many hours of reaction time, often over 250,000 times longer than predicted by Eq. (4). At the beginning of an experiment, [NO] immediately decreases due to physical adsorption, and then quickly (<0.2 h) increases to 164 ppm_v before approaching its maximum value (Figs. S4 and S7). The latter, more gradual increase in [NO] is attributed to Step 2 of the reaction mechanism; additional NO is being generated via NO_2 reduction at the carbon's surface. It is logical to assert, then, that the NO oxidation reaction achieves equilibrium during Step 1 quite rapidly, as might be predicted by Eq. (4). Any increase in [NO] over the steady-state value results from NO_2 reduction. As the surface saturates, NO_2 reduction slows, and [NO] re-approaches its steady-state value. NO oxidation (Step 1) is expected to achieve steady-state after <1 h, yet the system takes, in many cases, >24 h to achieve steady effluent [NO] and [NO_2]. These observations support that NO_2 adsorption/reduction (Step 2) controls the transient kinetics of NO oxidation. If pre-sorption of NO_2 is used to prevent further carbon surface reactions, then equilibrium (in this case, [NO] = 164 ppm_v and [NO_2] = 220 ppm_v) is achieved almost immediately (Fig. 4b).

To better understand and quantify NO generation from NO_2 reduction that occurs during NO oxidation, virgin ACFC-10 was treated with 220 ppm_v NO_2 following three protocols: (1) 220 ppm_v NO_2 in N_2 (NO_2), (2) 220 ppm_v NO_2 and 10 vol% O_2 in N_2 ($NO_2 + O_2$), and (3) 220 ppm_v NO_2 and 164 ppm_v NO in N_2 ($NO_2 + NO$) (Table 3, Fig. 5, and Table S1). 220 ppm_v is the NO_2 concentration for these experiments because we previously showed that for our representative NO oxidation conditions, 220 ppm_v of NO_2 is generated (Step 1 of reaction mechanism). Where applicable (i.e., for $NO + O_2$ and $NO_2 + NO$), a 164 ppm_v NO offset, representing the amount of unreacted NO during NO oxidation, is included in Fig. 5 to isolate the amount of NO released via NO_2 reduction. For each protocol, [NO] increases sharply to a peak value and then gradually decreases toward zero. NO_x adsorption capacity (Q_{ads}) was calculated for each protocol, and $Q_{ads}(NO_2) > Q_{ads}(NO_2 + O_2) \approx Q_{ads}(NO + O_2) > Q_{ads}(NO_2 + NO)$ (Table 3). For each protocol, the maximum [NO], after adjusting for inlet or unreacted [NO], is (NO_2, 134 ppm_v) > ($NO_2 + NO$, 129 ppm_v) > ($NO_2 + O_2$, 95 ppm_v) > ($NO + O_2$, 76 ppm_v).

NO_2 reduction is described by reaction (5). Stoichiometry is not included because of the complexity of the adsorbed species.

$$[NO_2] + \text{carbon} \rightarrow [NO]_{released} + -C(O) + -C(NO_x) \quad (5)$$

For protocols that include oxygen, re-oxidation of NO to NO_2 in the micropores may inhibit NO formation, explaining the lower [NO] for the $NO_2 + O_2$ scenario compared to the $NO_2 + N_2$ scenario (Fig. 5). Furthermore, in our baseline NO oxidation system ($NO + O_2$), equilibrium does not favor NO_2 reduction because unreacted NO is present [32], which is confirmed in the results for the NO_2 + NO scenario (Fig. 5). Scenarios that do not provide inlet NO favor NO_2 reduction, which is expected based on Le Chatelier's Principle. Additionally, NO_2 generated during NO oxidation is axially increasing along the carbon bed with 220 ppm_v in the outlet, causing the relatively low outlet [NO]. Understanding the role of each gas phase component can explain the differences in magnitude of [NO] and [NO_2] profiles during NO oxidation and NO_2 sorption.

4. Conclusions

NO oxidation catalyzed by microporous activated carbon occurs through two steps: (1) NO_2 is formed in activated carbon's micropores from reactions involving O_2 and NO, and (2) the formed NO_2 adsorbs/reacts with activated carbon's surface to generate NO and adsorbed species on the carbon. For the carbons tested here, stable physical properties result in constant steady-state NO oxidation kinetics associated with Step 1 of the reaction mechanism, regardless of the quantity of adsorbed species or oxygen surface functionalities. Step 2 determines the transient NO oxidation kinetics, including the amount of time necessary for the system to achieve steady effluent [NO] and [NO_2].

A virgin activated carbon requires additional time to reach steady conditions because it has a large number of unsaturated surface sites that can react with NO_2. A carbon pretreated with NO_2 or functionalized with oxygen has fewer or no reactive sites available and can achieve steady-state effluent NO and NO_2 concentrations more rapidly. It follows, then, that physical properties of the activated carbon catalyst control steady-state NO oxidation kinetics, while carbon's adsorption and surface reaction properties control transient kinetics. NO_2 sorption/reduction affects the transient NO oxidation kinetics only until the carbon surface is saturated with adsorbed nitrogen-containing species or oxygen functional groups. This work updates the reaction mechanism available in the literature, showing that NO is oxidized to NO_2 *before* the carbon adsorbs any NO_x species. Comparisons between NO oxidation and NO_2 sorption over activated carbon presented here are semi-quantitative and empirical. Theoretical studies, as well as additional experiments using other microporous catalysts, are underway to further support this mechanism. However, these results regarding the NO oxidation mechanism for microporous carbon provide an improved, fundamental understanding of NO oxidation kinetics as well as suggestions to more rapidly achieve steady-state – a problem that has challenged carbon-catalyzed NO oxidation studies in the past. Future research should build upon this work by focusing on Step 1 of the reaction mechanism to isolate the role of the catalyst's micropores in the NO oxidation mechanism.

Acknowledgements

Main project funding was provided by the National Science Foundation (NSF A1918 and NSF CBET 10-34470) and the National Natural Science Foundation of China (51008277). Support for Z. Zhang is provided by the Chinese Scholarship Council (2011645015). SEM, FTIR and XPS characterizations were carried out in part in the Frederick Seitz Materials Research Laboratory Central Facilities, University of Illinois at Urbana-Champaign, which are partially supported by the U.S. Department of Energy under grants DE-FG02-07ER46453 and DE-FG02-07ER46471.

Appendix A. Supplementary data

Supplementary material related to this article can be found, in the online version, at http://dx.doi.org/10.1016/j.apcatb.2013.10.050.

References

[1] Q. Wu, G. Mul, R. van de Krol, Energy & Environmental Science 4 (2011) 2140–2144.
[2] Z. Zeng, P. Lu, C. Li, L. Mai, Z. Li, Y. Zhang, Catalysis Science & Technology 2 (2012) 2188–2199.
[3] J.D. Felix, E.M. Elliott, S.L. Shaw, Environmental Science and Technology 46 (2012) 3528–3535.
[4] G. Qi, R.T. Yang, R. Chang, Applied Catalysis B: Environmental 51 (2004) 93–106.
[5] US Energy Information Adminstration, International Energy Outlook, 2011, pp. 2011.
[6] China Environmental Protection Agency, Emission Standard of Air Pollutants for Thermal Power Plants, 2011.
[7] Environmental Protection Agency (USA), Cross-State Air Pollution Rule (CSAPR), 2012.
[8] Y. Peng, J. Li, L. Chen, J. Chen, J. Han, H. Zhang, W. Han, Environmental Science and Technology 46 (2012) 2864–2869.
[9] J.H. Pavlish, E.A. Sondreal, M.D. Mann, E.S. Olson, K.C. Galbreath, D.L. Laudal, S.A. Benson, Fuel Processing Technology 82 (2003) 89–165.
[10] X. Gao, S. Liu, Y. Zhang, X. Du, Z. Luo, K. Cen, Catalysis Today 175 (2011) 164–170.
[11] Z. Wang, Y. Wang, D. Long, I. Mochida, W. Qiao, L. Zhan, X. Liu, S.-H. Yoon, L. Ling, Industrial and Engineering Chemistry Research 50 (2011) 6017–6027.
[12] I. Mochida, Y. Kawabuchi, S. Kawano, Y. Matsumura, M. Yoshikawa, Fuel 76 (1997) 543–548.
[13] I. Mochida, N. Shirahama, S. Kawano, Y. Korai, A. Yasutake, M. Tanoura, S. Fujii, M. Yoshikawa, Fuel 79 (2000) 1713–1723.
[14] I. Mochida, S. Kisamori, M. Hironaka, S. Kawano, Y. Matsumura, M. Yoshikawa, Energy and Fuels 8 (1994) 1341–1344.
[15] S. Adapa, V. Gaur, N. Verma, Chemical Engineering Journal (Lausanne) 116 (2006) 25–37.
[16] B. Galliker, R. Kissner, T. Nauser, W.H. Koppenol, Chemistry – A European Journal 15 (2009) 6161–6168.
[17] W.J. Zhang, S. Rabiei, A. Bagreev, M.S. Zhuang, F. Rasouli, Applied Catalysis B: Environmental 83 (2008) 63–71.
[18] J.D. Atkinson, Z. Zhang, M.J. Rood, 105th Annual Meeting of the Air & Waste Management Association, San Antonio, 2012, Paper 2012-A-2058-AWMA.
[19] J.D. Atkinson, Z. Zhang, Z. Yan, M.J. Rood, Carbon 54 (2013) 444–453.
[20] Z. Yan, Introduction to Catalysis, Press of Chemical Industry, Beijing, 2005.
[21] M. Bodenstein, Helvetica Chimica Acta 18 (1935) 743–759.
[22] W.-J. Zhang, A. Bagreev, F. Rasouli, Industrial and Engineering Chemistry Research 47 (2008) 4358–4362.
[23] S. Yang, J. Li, C. Wang, J. Chen, L. Ma, H. Chang, L. Chen, Y. peng, N. Yan, Applied Catalysis B: Environmental 117–118 (2012) 73–80.
[24] J. Després, M. Elsener, M. Koebel, O. Kröcher, B. Schnyder, A. Wokaun, Applied Catalysis B: Environmental 50 (2004) 73–82.
[25] J. Sun, S. Chen, M.J. Rood, M. Rostam-Abadi, Energy and Fuels 12 (1998) 1071–1078.
[26] Z. Hashisho, M.J. Rood, S. Barot, J. Bernhard, Carbon 47 (2009) 1814–1823.
[27] D. López, R. Buitrago, A. Sepúlveda-Escribano, F. Rodríguez-Reinoso, F. Mondragón, Langmuir 23 (2007) 12131–12137.
[28] E. Papirer, R. Lacroix, J.-B. Donnet, G. Nanse, P. Fioux, Carbon 32 (1994) 1341–1358.
[29] S. Sumathi, S. Bhatia, K.T. Lee, A.R. Mohamed, Journal of Hazardous Materials 176 (2010) 1093–1096.
[30] D. Kang, X. Tang, J. Peng, H. Yi, P. Ni, Z. Ye, K. Li, Advanced Materials Research 383–390 (2011) 3056–3062.
[31] X. Gao, S. Liu, Y. Zhang, Z. Luo, M. Ni, K. Cen, Fuel Processing Technology 92 (2011) 139–146.
[32] N. Shirahama, S.H. Moon, K.H. Choi, T. Enjoji, S. Kawano, Y. Korai, M. Tanoura, I. Mochida, Carbon 40 (2002) 2605–2611.
[33] N. Tang, Y. Liu, H. Wang, Z. Wu, Journal of Physical Chemistry C 115 (2011) 8214–8220.
[34] F. Liu, H. He, Journal of Physical Chemistry C 114 (2010) 16929–16936.
[35] J.P.S. Sousa, M.F.R. Pereira, J.L. Figueiredo, Applied Catalysis B: Environmental 125 (2012) 398–408.
[36] K. Barthelet, J. Marrot, D. Riou, G. Férey, Angewandte Chemie International Edition 114 (2002) 291–294.
[37] C.J. Tighe, M.V. Twigg, A.N. Hayhurst, J.S. Dennis, Industrial & Engineering Chemistry Research 50 (2011) 10480–10492.
[38] M.X. Wang, Z.H. Huang, K. Shen, F.Y. Kang, K.M. Liang, Catalysis Today 201 (2013) 109–114.

[39] T. Kyotani, A. Tomita, Journal of Physical Chemistry B 103 (1999) 3434–3441.
[40] A. Claudino, J.L. Soares, R.F.P.M. Moreira, H.J. José, Carbon 42 (2004) 1483–1490.
[41] P. Nowicki, H. Wachowska, R. Pietrzak, Journal of Hazardous Materials 181 (2010) 1088–1094.
[42] J. Zawadzki, M. Wiśniewski, K. Skowrońska, Carbon 41 (2003) 235–246.
[43] J. Zawadzki, M. Wiśniewski, Catalysis Today 119 (2007) 213–218.
[44] K. Kaneko, N. Fukuzaki, K. Kakei, T. Suzuki, S. Ozeki, Langmuir 5 (1989) 960–965.